THE STRESS DEVELOPMENT DURING FILAMENT WINDING OF THICK CYLINDERS

H. Thomas Hahn and S. S. Lee

August 1992

Prepared Under Grant No. N00014-91-J-4103

for

Office of Naval Research
800 North Quincy Street
Arlington, VA 22217-5000405
Attn: Dr. Yapa Rajapakse

Department of Engineering Science and Mechanics
The Pennsylvania State University
University Park, PA 16802

THE STRESS DEVELOPMENT DURING FILAMENT WINDING OF THICK CYLINDERS

H. Thomas Hahn and S. S. Lee
The Pennsylvania State University
University Park, PA 16802

ABSTRACT

The stress development during filament winding of thick composite cylinders has been studied using dry glass fiber tows. The thicknesses of the wound cylinders were more than 38 *mm* while the aluminum mandrel used had an outside diameter of 58 *mm*. Circumferential winding was used and the winding tension was varied between 4 and 23 *N*. The radial pressure measured at the mandrel surface using foil gages increased over the first 6 layers or so of winding, and then stayed constant or even decreased slightly with subsequent winding. Predictions based on elastic analyses were fitted to the data by varying the effective radial modulus. The resulting values of the radial modulus were much less than the circumferential modulus, the latter being more than ten-thousand times greater than the former. Such high anisotropy was responsible for the asymptotic increase of the mandrel pressure with winding. The calculated circumferential stress in the fibers was compressive throughout most of the inner part of the wound cylinder; however, its magnitude was rather small. A higher winding tension resulted in a better compaction, and therefore, a smaller effective layer thickness, a higher radial modulus, and higher internal stresses. Under the winding conditions studied in the present work, fiber buckling due to the development of compressive circumferential stress does not appear possible.

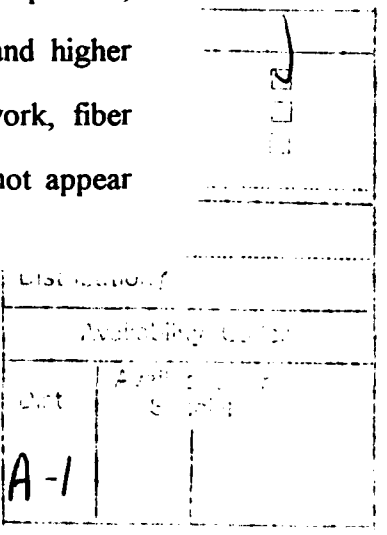

INTRODUCTION

Filament winding is a manufacturing process ideally suited for fabricating composite cylinders. Although originally developed for thin shells, it could be used for thick shells as well if proper processing conditions can be found. One of the major problems with filament winding thick cylinders is the fiber wrinkling that could result from fibers being under compression.

In filament winding, continuous bands of resin impregnated fibers are wound onto a rotating mandrel along predetermined paths. The winding angle may vary from longitudinal to circumferential to meet the structural requirements and processing limitations.

Depending on the method of resin impregnation, there are in general two type of filament winding: dry winding and wet winding. Dry winding utilizes fiber tows preimpregnated with B-staged resin. In wet winding, resin impregnation is performed on line by pulling the fiber tows through a liquid resin bath during winding.

A tensile force, called the winding tension, is usually applied to the fiber tow to ensure that the tow is placed on the right path without fiber buckling and also to enhance radial fiber compaction. However, a tow freshly laid under tension exerts a radial pressure on the previously wound tows. As additional layers of tows are wound, the inside fibers may eventually come under compression in their axial direction. In thick composites, the compressive stress may be high enough to induce fiber buckling. Also, under winding tension, fibers can migrate radially inward by replacing the viscous resin. Such fiber movement will of course change the stress distribution with time. Thus the residual stress distribution inside the cylinder will depend not only on the winding tension but also on the resin viscosity.

In dry winding, the relaxation of fiber tension will take a longer time because the B-staged resin has a much higher viscosity than the liquid resin. Even in wet winding, fibers should be immersed in a sufficient amount of resin to be able to move radially

inward if much stress relaxation is to occur. In an ideal winding, the amount of resin and its viscosity should be such that enough winding tension can be applied to remove voids and gaps. Yet the fiber tension must be fully relaxed by the end of the processing. It should be noted that the relaxation of the fiber tension is the result of the fibers moving inward radially, thereby reducing their length. Being elastic, the fibers themselves have no capability to creep.

After winding, the mandrel-composite assembly is heated in an oven or autoclave to the cure temperature. If the mandrel has a higher coefficient of thermal expansion than the composite, which is usually the case with aluminum or steel mandrels, it will push the composite layers outward radially and subsequently induce tension in the fibers nearby. As the temperature increases, the resin viscosity decreases to allow further fiber movements until it starts to increase again with advancing cure.

When cure is complete, the assembly is cooled down to ambient temperature and the composite cylinder is removed from the mandrel. The internal radial stress induced by the temperature change is tensile because of the anisotropy of the composite. An additional tensile stress may be induced by the excessive shrinkage of the mandrel.

Stress distributions and their implications on the structural integrity of thick filament- wound cylinders have been described in detail by Tarnopol'skii and Beil' [1]. They pointed out that the radial modulus is much lower than the circumferential modulus, and as a result, fibers can be subjected to axial compression especially in thick cylinders. Four different models were used to describe the radial compressibility: linear elastic, piecewise linear elastic, nonlinear, and viscoelastic. When proper values were used, the linear elastic model was shown to describe all the key features of the stress distribution rather well. They also discussed the importance of additional stress due to curing and mandrel removal.

Reuter [2] analyzed the radial stress development in a thin cylinder at various stages of filament winding. Filament winding was divided into the following stages:

winding, application of autoclave pressure, heating to the cure temperature, layer movement, cooling to room temperature, pressure removal, and mandrel removal. The linear elasticity theory was used throughout the analysis.

While references [1] and [2] were concerned with the stress development only, the problems of heat transfer, resin flow and curing were additionally addressed by a number of researchers [3-6]. The heat transfer analysis included the production of heat as a result of exothermic curing and the resin flow analysis made use of the Darcy's law. A reaction rate type of equation was used to describe the cure kinetics.

As far as winding-induced stresses are concerned, an analogy can be drawn between filament winding and tape winding. Assuming that the tape reel could be characterized as linearly elastic, Altmann [7] derived a set of integral equations, which are essentially the same as those in [1], to predict interlayer pressure and in-roll tension. Monk et al. [8] reproduced Altmann's analysis and examined in more detail the effect of various winding tension profile on the stress distribution. Crimping or buckling of the tape in the reel due to circumferential compression was highlighted. Yagoda [9] examined the influence of hub compliance on the in-roll stress distribution. Based largely on Altmann's result, Yagoda derived a closed-form solution using an infinite series expansion.

Although the stress development in filament winding has been studied by a number of researchers, no definitive analysis-experiment correlation has been established. One of the reasons is the lack of appropriate experimental data for the input properties. Also, a more realistic analysis is no longer linear.

The present paper describes the results of a study to investigate the stress development during winding of a dry glass fiber tow on a circular cylinder. The main objective was to find out whether or not fiber buckling was possible during dry winding of thick cylinders. Analysis-experiment correlation was used iteratively to gain a better insight into the winding and material parameters that affect the stress development.

ANALYSIS

Consider a continuous fiber tow of width w and thickness t being wound onto a circular mandrel in the circumferential direction. The inner and outer radii of the mandrel are denoted by a_m and b_m, respectively, Fig. 1. Suppose k layers have already been wound and the next $(k+1)$th layer is being wound under a winding tension T. The inner and outer radii of the kth layer are denoted by a_k and b_k respectively. Thus the inner radius of the wound cylinder is a_1, which is equal to b_m.

The radial pressure $p_o^{(k)}$ on the wound cylinder exerted by the $(k+1)$th layer is given by

$$p_o^{(k)} = \frac{T}{w b_k} \tag{1}$$

The stresses σ_r, σ_θ, and the radial displacement u induced by the winding of the $(k+1)$th layer are obtained from a plane-stress solution for a cylindrically orthotropic ring as [1]:

(1) Wound cylinder, $a_1 \le r \le a_k$,

$$\sigma_r^{(k)} = \frac{p_i^{(1)} c_k^{\beta+1}}{1 - c_k^{2\beta}}\left[\left(\frac{r}{b_k}\right)^{\beta-1} - \left(\frac{r}{b_k}\right)^{-\beta-1}\right] - \frac{p_o^{(k)}}{1 - c_k^{2\beta}}\left[\left(\frac{r}{b_k}\right)^{\beta-1} - c_k^{2\beta}\left(\frac{r}{b_k}\right)^{-\beta-1}\right] \tag{2}$$

$$\sigma_\theta^{(k)} = \frac{p_i^{(1)} c_k^{\beta+1}\beta}{1 - c_k^{2\beta}}\left[\left(\frac{r}{b_k}\right)^{\beta-1} + \left(\frac{r}{b_k}\right)^{-\beta-1}\right] - \frac{p_o^{(k)}\beta}{1 - c_k^{2\beta}}\left[\left(\frac{r}{b_k}\right)^{\beta-1} + c_k^{2\beta}\left(\frac{r}{b_k}\right)^{-\beta-1}\right] \tag{3}$$

$$u^{(k)} = \frac{p_i^{(1)} c_k^{\beta+1} b_k}{E_\theta (1 - c_k^{2\beta})} \left[(\beta - v_{\theta r}) \left(\frac{r}{b_k} \right)^{\beta} + (\beta + v_{\theta r}) \left(\frac{r}{b_k} \right)^{-\beta} \right]$$
$$- \frac{p_o^{(k)} b_k}{E_\theta (1 - c_k^{2\beta})} \left[(\beta - v_{\theta r}) \left(\frac{r}{b_k} \right)^{\beta} + (\beta + v_{\theta r}) \left(\frac{r}{b_k} \right)^{-\beta} \right] \tag{4}$$

(2) Mandrel, $a_m \le r \le b_m$,

$$(\sigma_r^{(k)})_m = - \frac{p_o^{(m)} b_m^2}{b_m^2 - a_m^2} \left(1 - \frac{a_m^2}{r^2} \right)$$
$$(\sigma_\theta^{(k)})_m = - \frac{p_o^{(m)} b_m^2}{b_m^2 - a_m^2} \left(1 + \frac{a_m^2}{r^2} \right) \tag{5}$$
$$(u^{(k)})_m = - \frac{p_o^{(m)} b_m^2 r}{E_m (b_m^2 - a_m^2)} \left[(1 - v_m) + (1 + v_m) \frac{a_m^2}{r^2} \right]$$

(3) New layer, $a_k \le r \le a_{k+1}$

$$(\sigma_r^{(k+1)})_o = \frac{p_o^{(k)} c_{k+1}^{\beta+1}}{1 - c_{k+1}^{2\beta}} \left[\left(\frac{r}{b_{k+1}} \right)^{\beta-1} - \left(\frac{r}{b_{k+1}} \right)^{-\beta-1} \right]$$
$$(\sigma_\theta^{(k+1)})_o = \frac{p_o^{(k)} c_{k+1}^{\beta+1} \beta}{1 - c_{k+1}^{2\beta}} \left[\left(\frac{r}{b_{k+1}} \right)^{\beta-1} + \left(\frac{r}{b_{k+1}} \right)^{-\beta-1} \right] \tag{6}$$
$$(u^{(k+1)})_o = \frac{p_o^{(k)} c_{k+1}^{\beta+1} b_{k+1}}{E_\theta (1 - c_{k+1}^{2\beta})} \left[(\beta - v_{\theta r}) \left(\frac{r}{b_{k+1}} \right)^{\beta} + (\beta + v_{\theta r}) \left(\frac{r}{b_{k+1}} \right)^{-\beta} \right]$$

In the above equations, E and ν are the Young's modulus and Poisson's ratio, respectively, and $c_k = a_1 / b_k$. The radial pressure on the mandrel surface $p_i^{(1)}$, called the mandrel pressure, is determined from the displacement continuity condition

$$u^{(k)} = (u^{(k)})_m \qquad at \quad r = a_1 = b_m \tag{7}$$

The resultant stresses and radial displacement in a filament-wound cylinder consisting of N layers are then obtained by summing up those induced by winding of each layer. The final results are:

(1) Wound cylinder, $a_p \le r \le b_p$

$$\begin{aligned} \sigma_r &= \sum_{k=p}^{N-1} \sigma_r^{(k)} + (\sigma_r^{(p)})_o \\ \sigma_\theta &= \sum_{k=p}^{N-1} \sigma_\theta^{(k)} + (\sigma_\theta^{(p)})_o \\ u &= \sum_{k=p}^{N-1} u^{(k)} + (u^{(p)})_o \end{aligned} \tag{8}$$

(2) Mandrel, $a_m \le r \le b_m$

$$\begin{aligned} (\sigma_r)_m &= \sum_{k=1}^{N-1} (\sigma_r^{(k)})_m \\ (\sigma_\theta)_m &= \sum_{k=1}^{N-1} (\sigma_\theta^{(k)})_m \\ (u)_m &= \sum_{k=1}^{N-1} (u^{(k)})_m \end{aligned} \tag{9}$$

It should be noted that the final mandrel pressure p_m is equal to $-(\sigma_r)_m$ at $r = b_m$.

EXPERIMENTAL PROCEDURE

Filament winding was carried out on a McClean Anderson 3-axis filament winder using E-glass fiber tows. The fibers, whose nominal diameter was 13 μm, had a silane sizing with uncured epoxy finish. The fiber tow had 7 bundles, each bundle containing 700 filaments. The tow was nominally 3.3 *mm* wide and 0.23 *mm* thick.

The fiber tow was wound on an aluminum mandrel over its 50-*mm* mid section which was bounded by a pair of end plates. The mandrel was 57.7 *mm* in outside diameter, 3.4 *mm* thick, and 203 *mm* long. The end plates were fitted onto the mandrel to prevent the wound tow from slipping, Fig. 2. These end plates were machined out of transparent plexiglass sheets to enable on-line monitoring of fiber buckling at an edge. A video camera was used to record the winding process for later examination, Fig. 3.

Winding tension was applied using an American Sahm tensioner. It was varied between 4 and 23 *N*. However, in each winding series the winding tension was kept constant throughout. A full layer of winding required 15.4 revolutions of the mandrel to minimize gaps and laps. Winding continued until more than 100 layers were wound.

Wire-based pressure gages from Interlink Electronics were used to measure the mandrel pressure. Four gages were attached on the mandrel surface equal distances apart along the circumference, Fig. 2. The gages were 15 *mm wide*, 23 *mm long*, 0.3 *mm* thick, and had a 10-*mm* diameter active area. They were designed for pressures up to 210 *kPa*. The system configuration used for data acquisition is shown schematically in Fig. 3.

RESULTS AND DISCUSSION

The effective layer thickness, i.e., the cylinder thickness divided by the total number of layers, decreased with increasing winding tension, Fig. 4. In other words, a tighter winding resulted in a thinner cylinder for the same number of layers. From the number of filaments in the tow, the effective fiber volume fractions were calculated, and the results are shown in Fig. 5.

A typical change of the mandrel pressure with the number of layers wound is shown in Fig. 6. Note that time, instead of the layer number, has been used on the abscissa. Some stress relaxation is seen at long times. The stress relaxation continued somewhat even after winding.

The pressure increase in Fig. 6 is stepwise because the pressure does not increase until the gage comes into contact with the tow. Note that the tow is only 3.3 *mm* wide whereas the winding area is 50 *mm* long. It takes a while before a full coverage is achieved. However, the full coverage of the gages by the tow takes place rather quickly because the gages are small. The pressure then stays constant until next contact occurs. The stepwise increase of the mandrel pressure can be more clearly seen in Fig. 7, which is an expanded view of the initial winding after time has been converted to a layer number.

The variation in the measurements from gage to gage is substantial. Furthermore, the mandrel pressure after the first layer is wound should be 10.5 *kPa* for every Newton of winding tension, see Eq. (1). However, the predictions are higher than the measured in all winding series, Fig. 8. The reason is that, unlike liquid, fibers come into contact with the gage at discrete points, which seems to give lower readings. Furthermore, the degree of contact is likely to vary from gage to gage depending on many factors such as the position of the gage and the local shape of the tow.

To minimize the gage-to-gage variability and to compensate for the lower-than-expected gage sensitivity, the data were normalized with respect to the mandrel pressure after the first layer. Unfortunately, the normalization still could not eliminate the gage variability entirely. Nevertheless, the gage sensitivity could be accounted for.

The normalized mandrel pressure under a winding tension of 4.45 *N* is shown as a function of the number of layers wound in Fig. 9. After only 3 or 4 layers are wound, the pressure does not increase any more. The reason is that the winding tension is taken up by the fibers mostly as the circumferential stress.

The mandrel pressure was calculated using the equations developed earlier. The input properties used are listed in Table 1. Layer thicknesses and fiber volume fractions were taken from Figs. 4 and 5, respectively. The circumferential modulus was taken as the product of the fiber modulus and the fiber volume fraction. The Poisson's ratio was the same as that of the glass fiber. Since the radial modulus was not known *a priori*, it

was varied until a reasonable fit was obtained with the experimental data. The resulting prediction is shown as a solid curve in Fig. 9. The deduced radial modulus is only 0.90 *MPa*, compared with 38.42 *GPa* for the circumferential modulus. An extremely high anisotropy is thus found to exist in the wound cylinder.

The experimental data for winding tensions up to 22.27 *N* were analyzed similarly, and the results are shown in Figs. 10 through 13. In all cases a reasonable agreement is seen between the prediction and the experiment when the radial modulus is chosen properly. Within the range of winding tension studied, no further increase in the mandrel pressure is seen after only 6 layers have been wound.

With the use of the deduced values of the radial modulus, the circumferential stress distribution in a 100-layer cylinder was calculated and the results are shown in Figs. 14 through 18. Regardless of the winding tension, the circumferential stress remains compressive throughout most of the inner region of the cylinder. It becomes tensile only near the outer surface and near the mandrel. The magnitude of the maximum compressive stress increases with the winding tension. However, even under the maximum winding tension of 22.27 *N*, the compressive circumferential stress is only 0.24 *MPa*. Thus, fiber buckling is not likely. This conclusion is in agreement with experimental observations, where one edge of the cylinder was monitored during winding for any sign of fiber buckling.

The radial pressure, i.e., the negative radial stress, in a 100-layer cylinder wound under a 22.27-*N* winding tension is shown in Fig. 19. Near the mandrel, the radial pressure decreases rapidly with distance away from the mandrel. However, it stays fairly constant over a large inner region until the outer surface is reached. The pressure then decreases rapidly again over a thin surface region. The radial pressure that most of the inner region is subjected to is less than 0.25 *MPa* and a good consolidation is expected to be difficult to achieve under the winding tension used.

The change of circumferential stress distribution with the number of layers in the cylinder is shown in Fig. 20. When there are only 5 layers in the cylinder, the circumferential stress remains tensile throughout the entire thickness of the cylinder. As the number of layers increases to 10, the inner layers begin to be subjected to circumferential compression. Thus, fiber buckling during filament winding is possible only in thick cylinders where circumferential stress could become compressive.

CONCLUSIONS

During filament winding of circular cylinders, stresses develop because of the winding tension applied to the fiber tows to improve compaction. In the present study a glass fiber tow and an aluminum mandrel were used to study the stress development in the filament winding of more than 100 layers..

As expected, compaction increased with increasing winding tension. Consequently, both the effective fiber volume fraction and the effective radial modulus increased. The pressure on the mandrel surface was measured using foil-type pressure gages and the result was used in the analysis-experiment correlation to determine the effective radial modulus. The deduced radial modulus was found to be several orders of magnitude smaller than the circumferential modulus.

The high anisotropy prevented the mandrel pressure from increasing continuously with the number of layers. There was no significant increase in the mandrel pressure after only about 6 layers had been wound. Since much of the winding tension had to be borne by the fibers in circumferential direction, the circumferential stress was compressive in most of the inner region of the thick cylinder. Its magnitude, although small, increased with increasing winding tension. Nevertheless, no apparent fiber buckling was observed during winding.

The probability of fiber buckling inside the wound cylinder increases with increasing compressive circumferential stress but with decreasing radial modulus. Since

the winding tension increases both the circumferential stress and the radial modulus, an optimum value may exist which can minimize the probability of fiber buckling during filament winding of thick cylinders.

REFERENCES

1. Tarnopol'skii, Y.M. and Beil', A.I., " Problems of the Mechanics of Composite Winding," Chapter II in *Handbook of Composites, Vol. 4: Fabrication of Composites*, A. Kelly and S.T. Mileiko, Eds., Elsevier Science Publisher B.V., 1983, p.45.

2. Reuter, R.C. Jr., " Prediction and Control of Macroscopic Fabrication Stresses in Hoop Wound, Fiberglass Rings," *Analysis of the Test Methods for High Modulus Fibers and Composites, ASTM STP 521*, American Society for Testing Materials, 1973, p.264.

3. Spencer, B.E., " Prediction of Manufacturing Stresses in Thick-walled Orthotropic Cylinder," Ph.D. Thesis, The University of Nebraska-Lincoln, 1988.

4. Tzeng, J.T.S. and Loos, A.C.," A Model of the Winding and Curing Processes for Filament Wound Composites," Report CCMS-89-01, Virginia Polytechnic Institute and State University, 1988.

5. Calius, E.P. and Springer, G.S.," Modeling the Filament Winding Process," *Proceedings of Fifth International Conference on Composite Materials (ICCM-V)*, 1985, p.1071.

6. Cai, Z., Gutowski, T., and Allen, S., " Winding and Consolidation Analysis for Cylindrical Composite Structures," to be published in *Journal of Composite Materials*.

7. Altmann, H.C., "Formulas for Computing the Stresses in Center-Wound Rolls," *Journal of the Technical Association of the Pulp and Paper Industry (TAPPI)*, Vol. 51, 1968, p.176.

8. Monk, D.W., Lautner, W.K., and McMullen, J.F., " Internal Stresses Within Rolls of Cellophane," *TAPPI*, Vol. 58, , 1975, p. 152.

9. Yagoda, H.P., " Resolution of a Core Problem in Wound Rolls, " *ASME Journal of Applied Mechanics*, Vol. 47, 1980, p.847.

Table 1. Effective material properties

Composite

Property	Winding Tension, N				
	4.45	8.91	13.36	17.82	22.27
E_θ, GPa	38.42	46.40	56.55	65.24	65.24
$\nu_{\theta r}$	0.22	0.22	0.22	0.22	0.22
E_r, MPa	0.90	1.17	1.24	1.31	1.45
V_f	0.53	0.64	0.78	0.90	0.90
Thickness, μm	427	354	290	226	224

Mandrel

$$E_m = 68.95\,GPa, \qquad \nu_m = 0.33$$

$$a_m = 25.4\,mm, \qquad b_m = 28.8\,mm$$

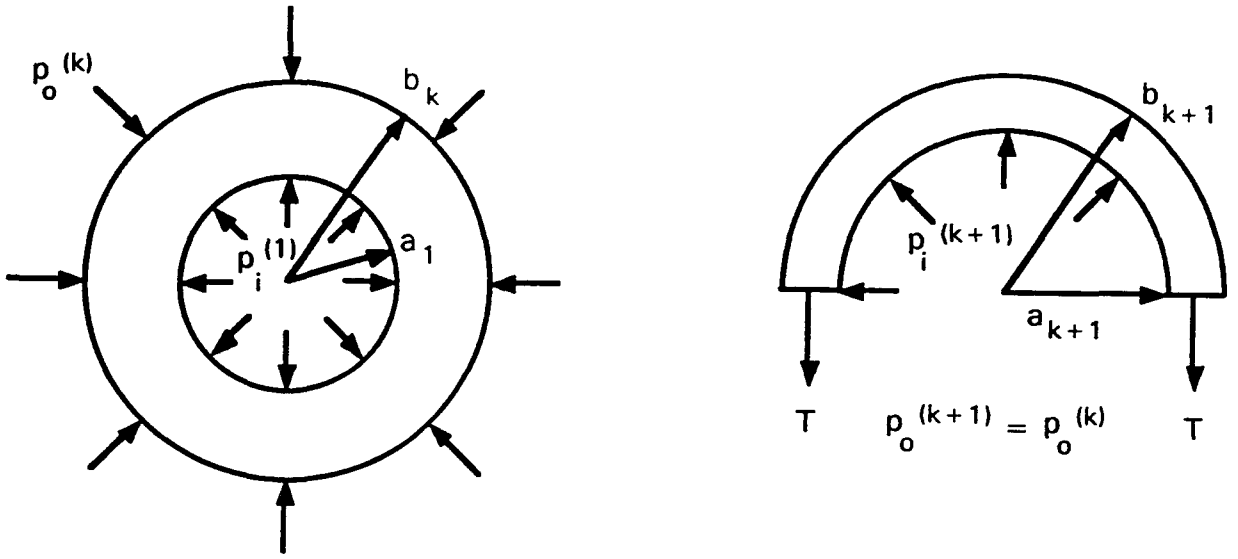

Composite

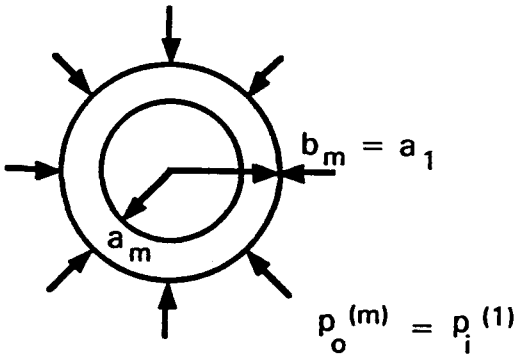

Mandrel

Fig. 1. Three components for stress analysis

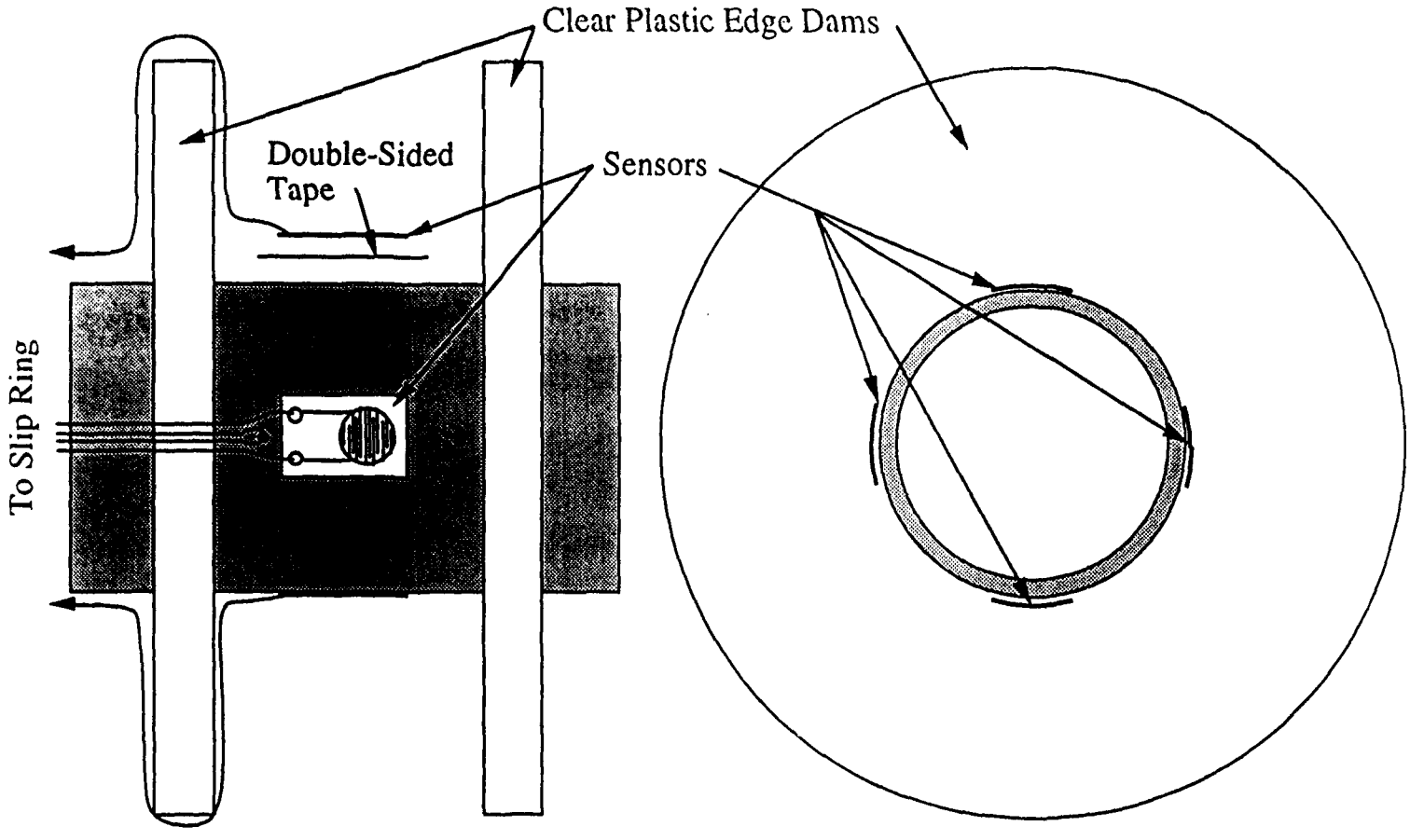

Fig. 2. Mandrel/sensor arrangement

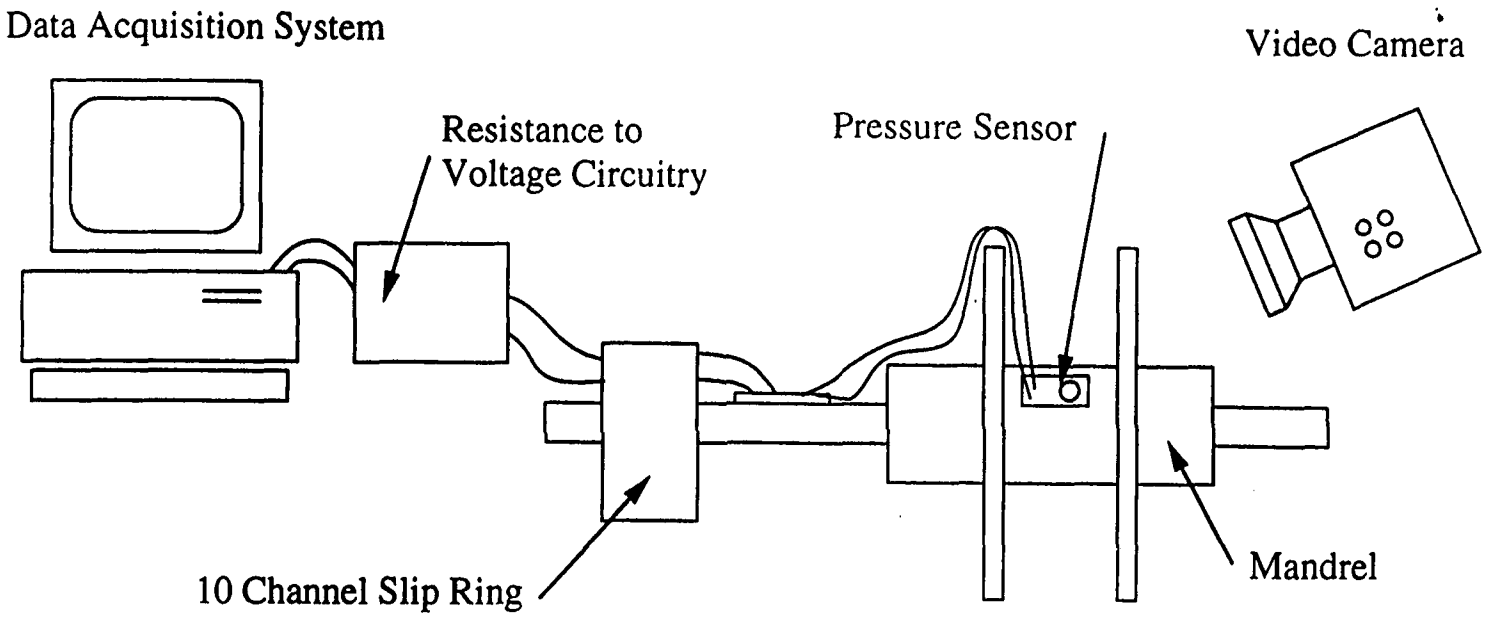

Fig. 3. Experimental setup for visualizing the development of wavy layers

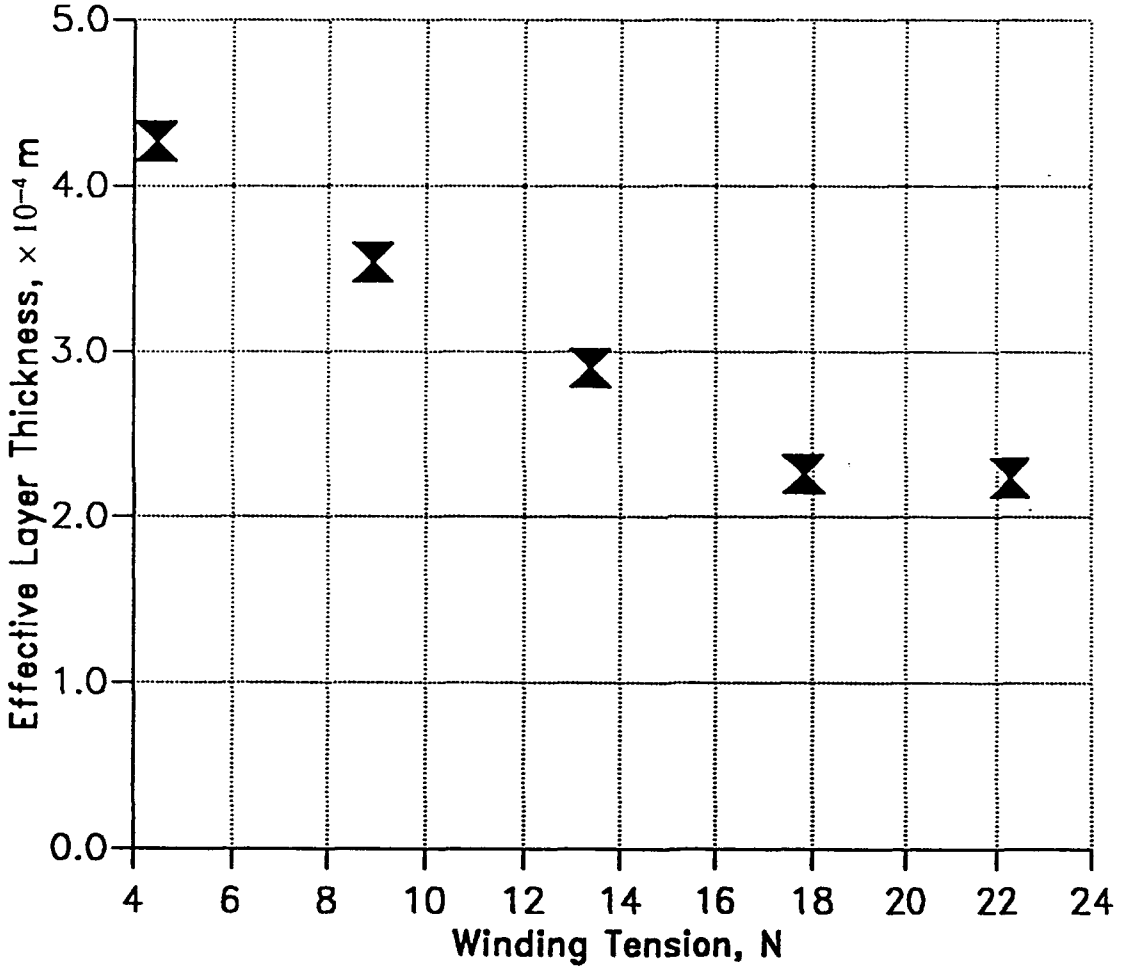

Fig. 4. Change of effective layer thickness with winding tension

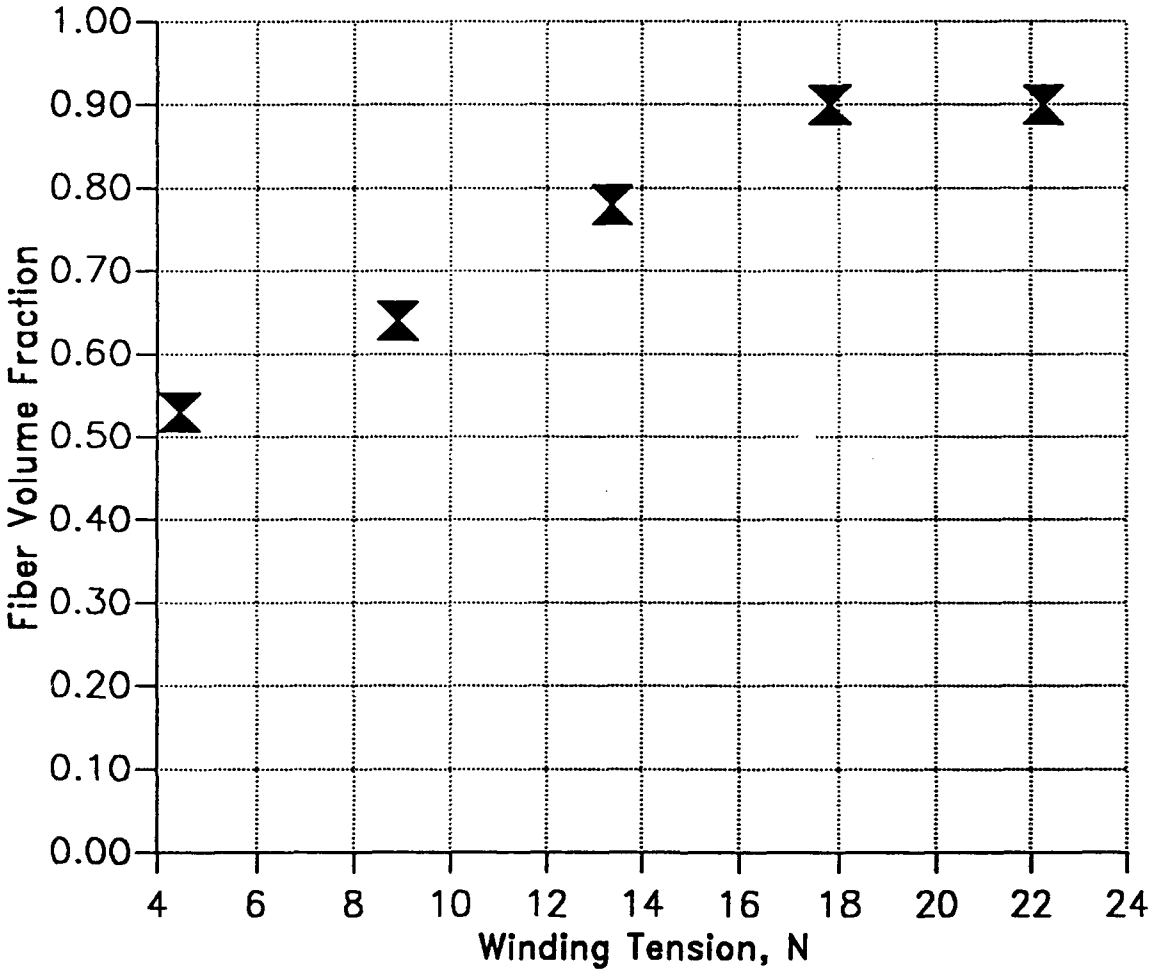

Fig. 5. Change of fiber volume fraction with winding tension

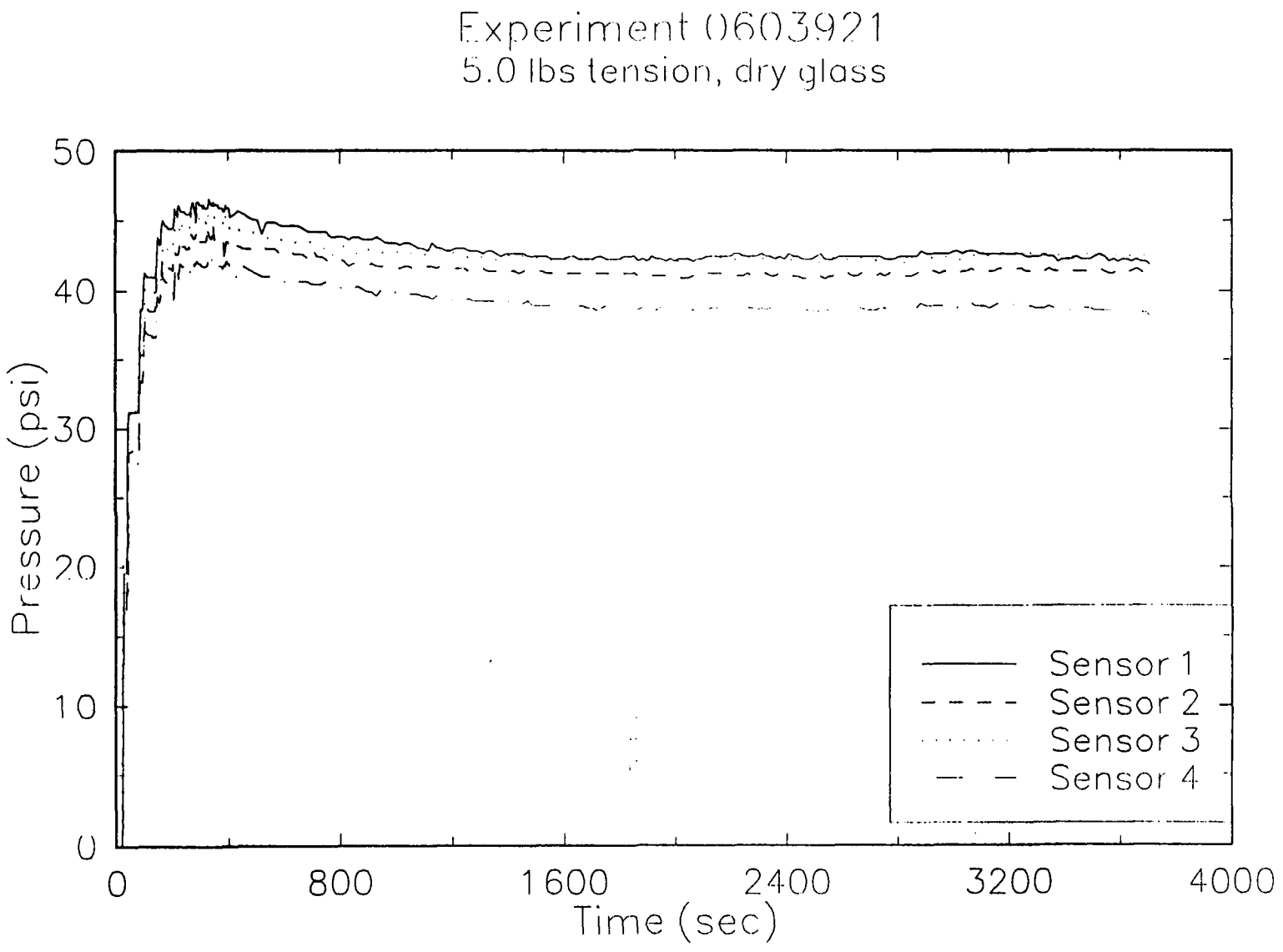

Fig. 6. Change of mandrel pressure with winding time

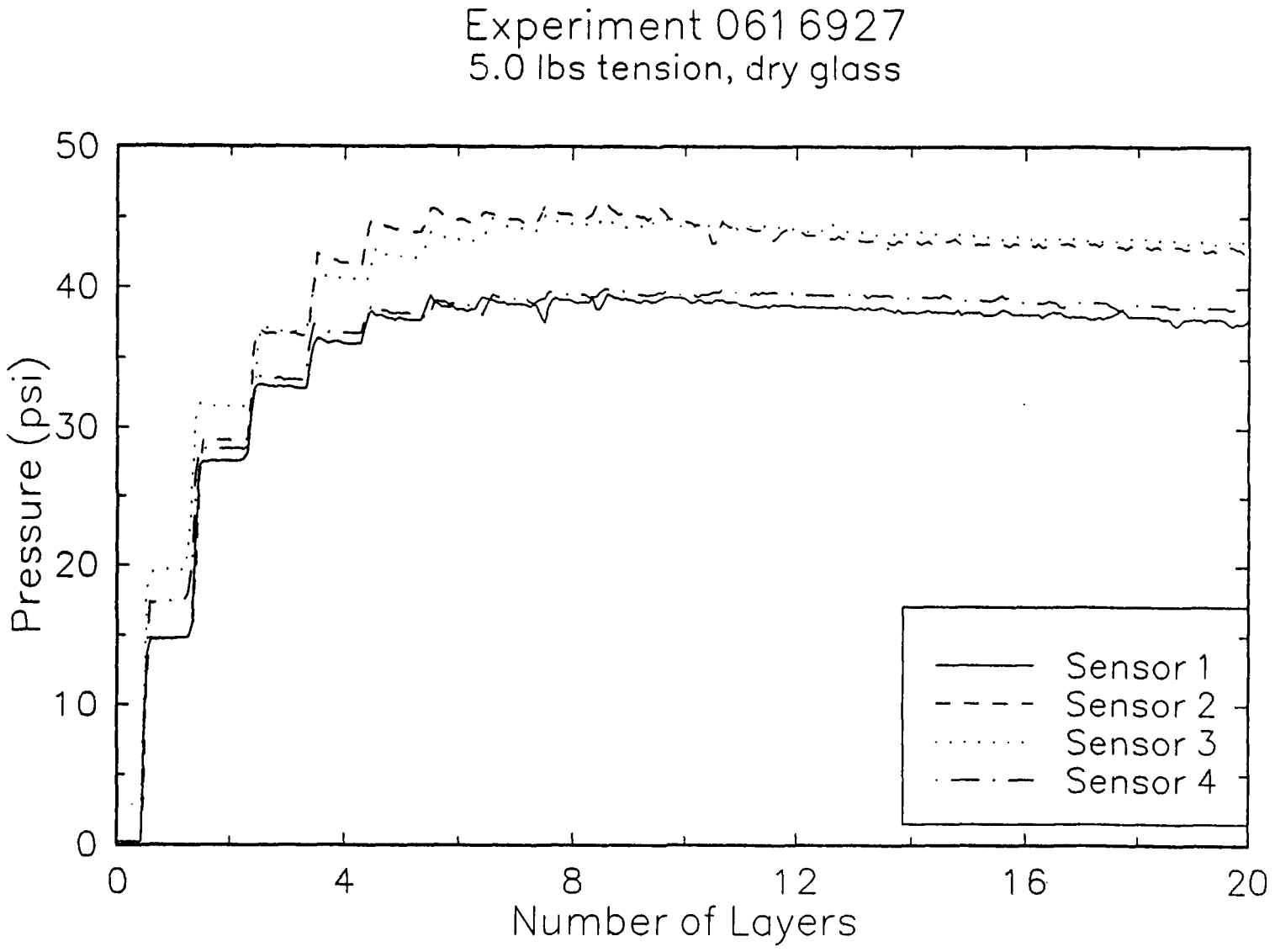

Fig. 7. Change of mandrel pressure with number of layers wound

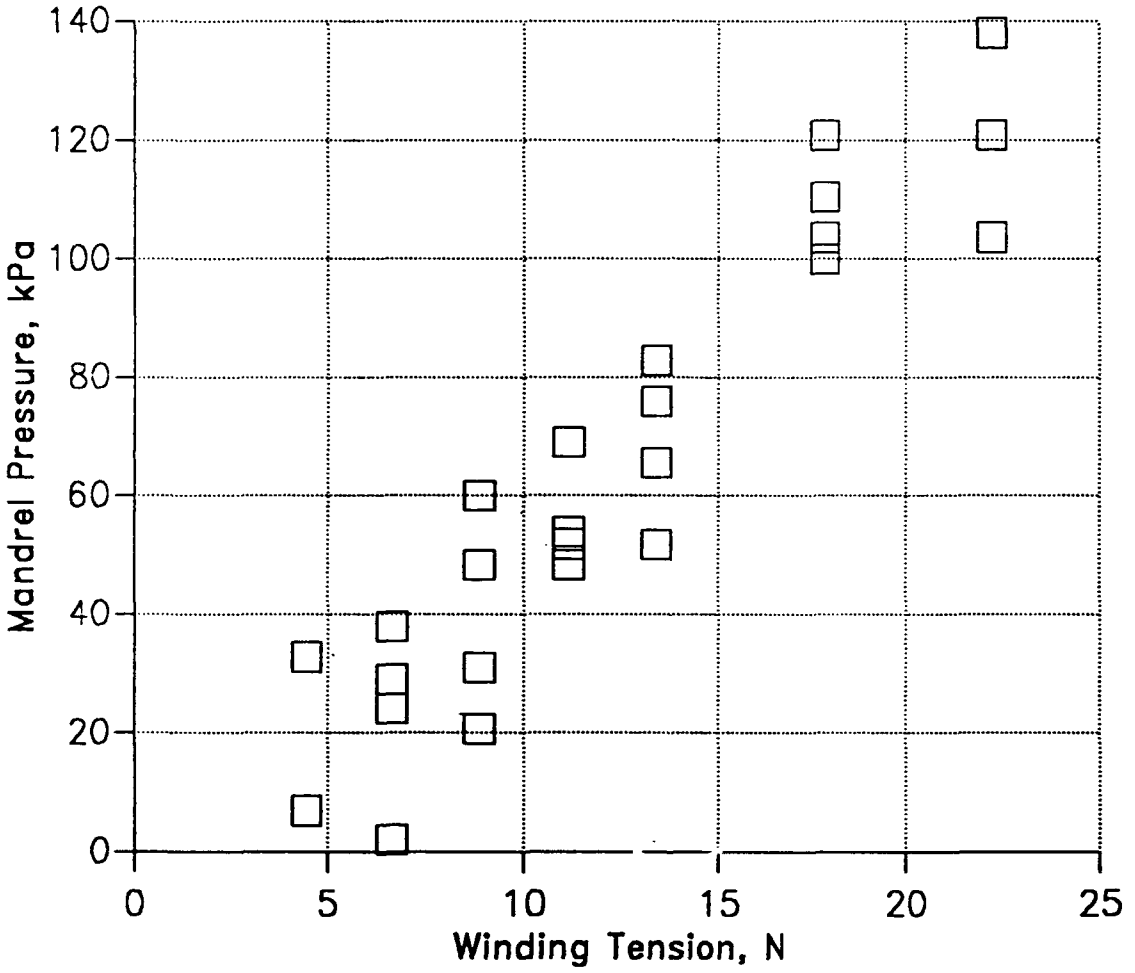

Fig. 8. Mandrel pressure after first layer wound.

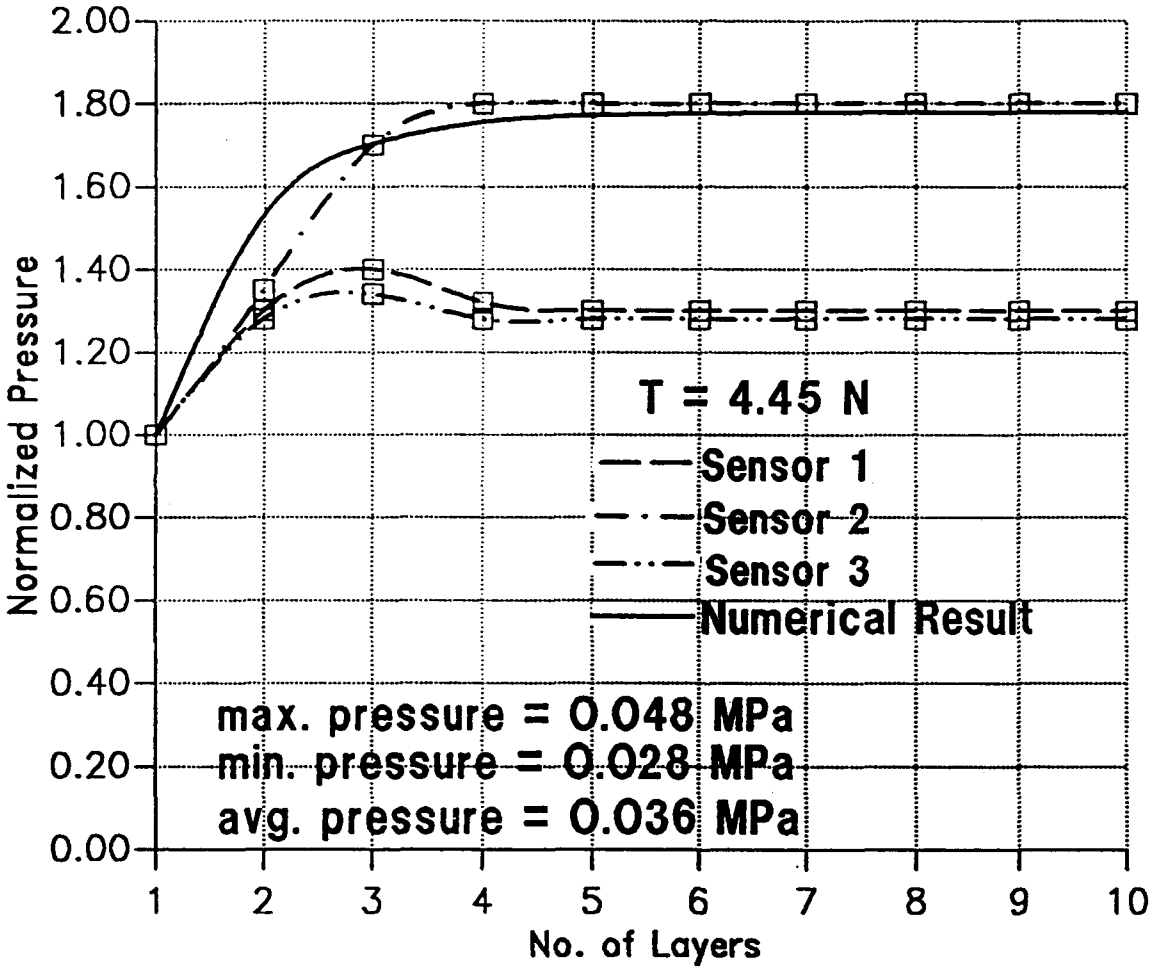

Fig. 9. Change of normalized mandrel pressure with number of layers wound, winding tension = 4.45 N

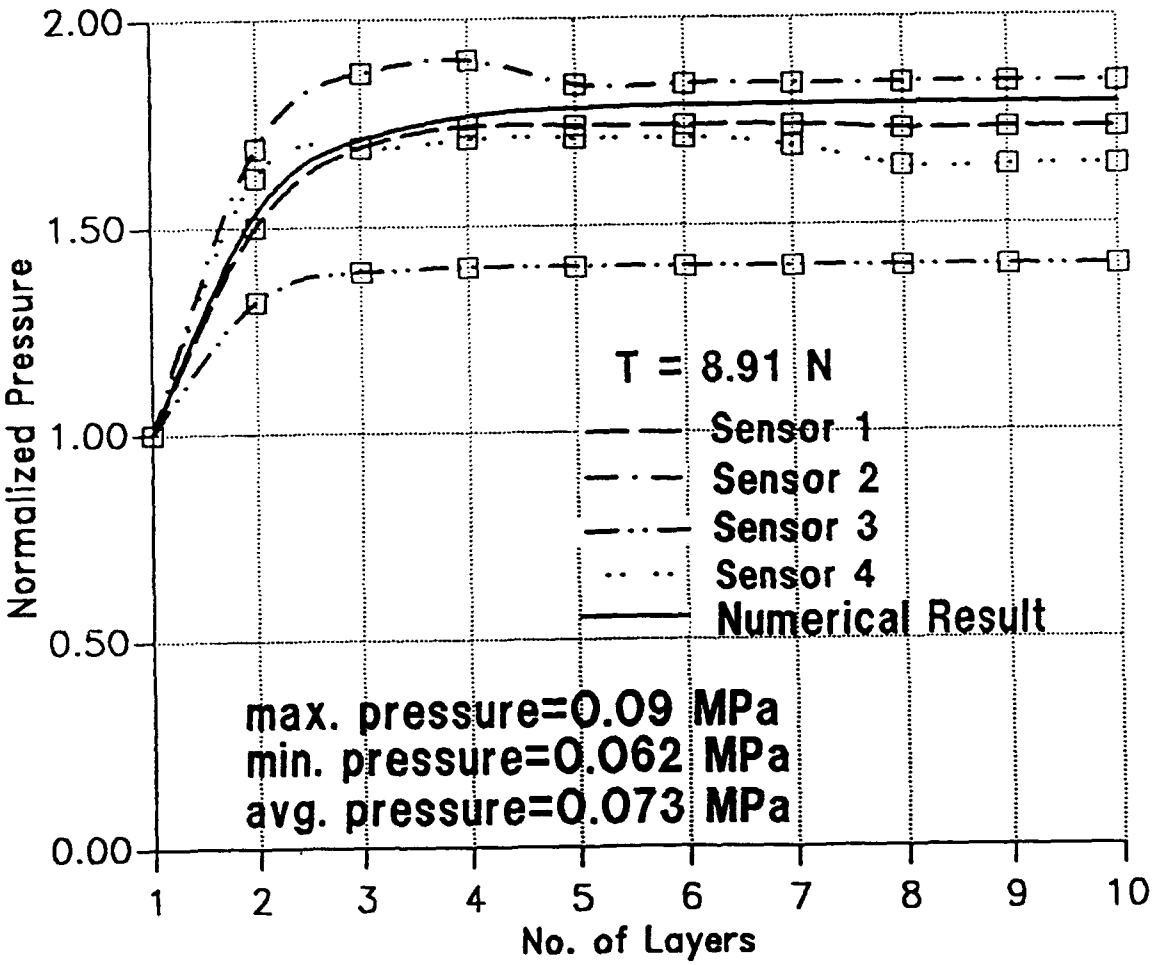

Fig. 10. Change of normalized mandrel pressure with number of layers wound, winding tension = 8.91 N

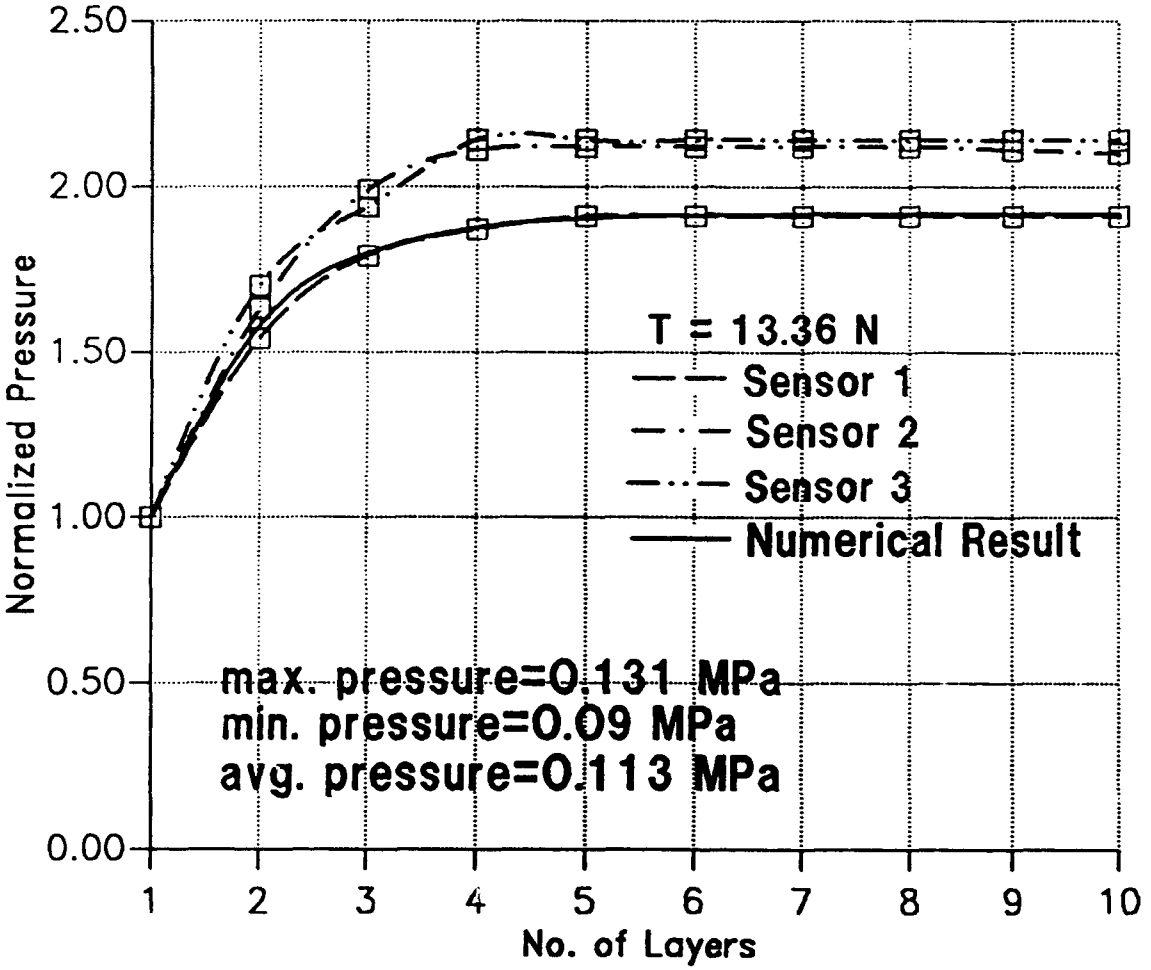

Fig. 11. Change of normalized mandrel pressure with number of layers wound, winding tension = 13.36 N

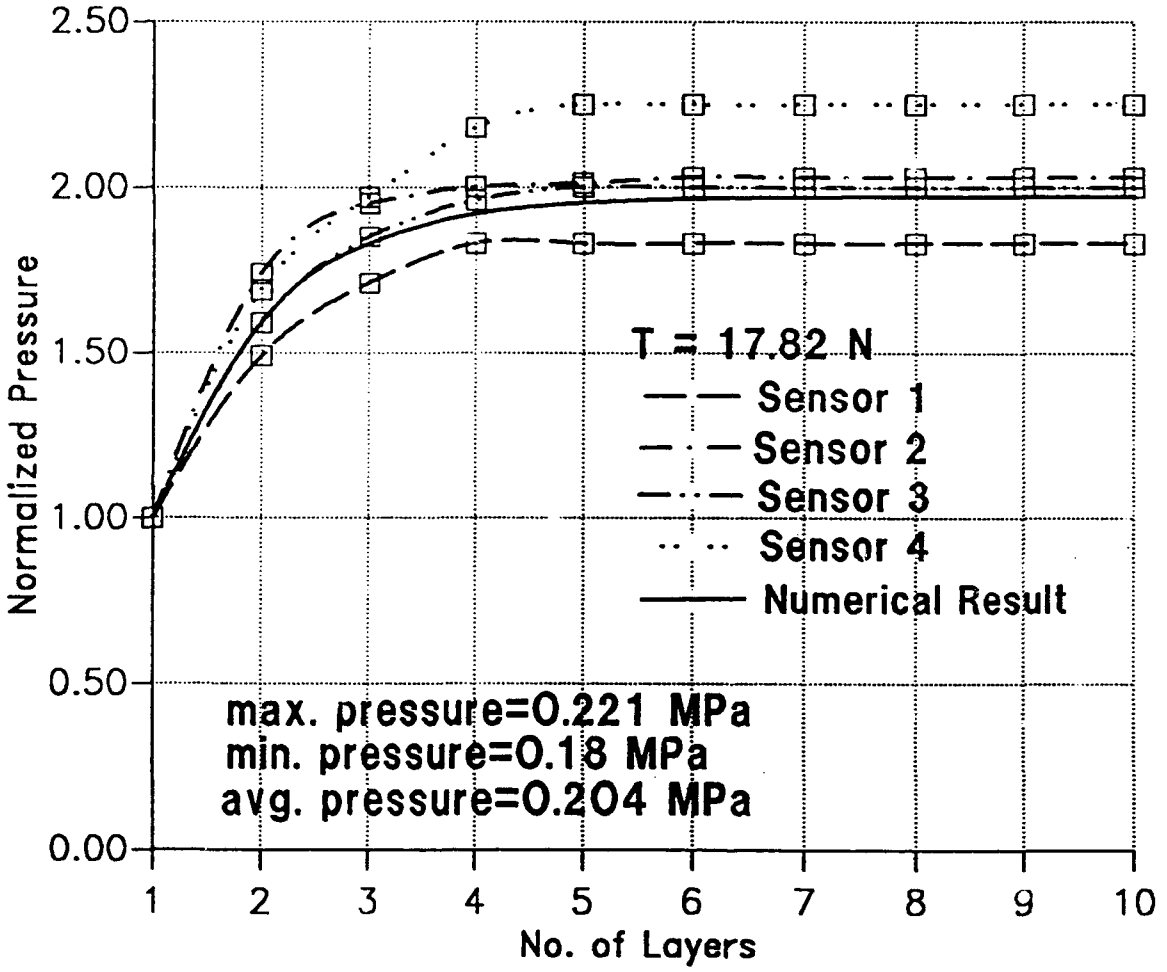

Fig. 12. Change of normalized mandrel pressure with number of layers wound, winding tension = 17.82 N

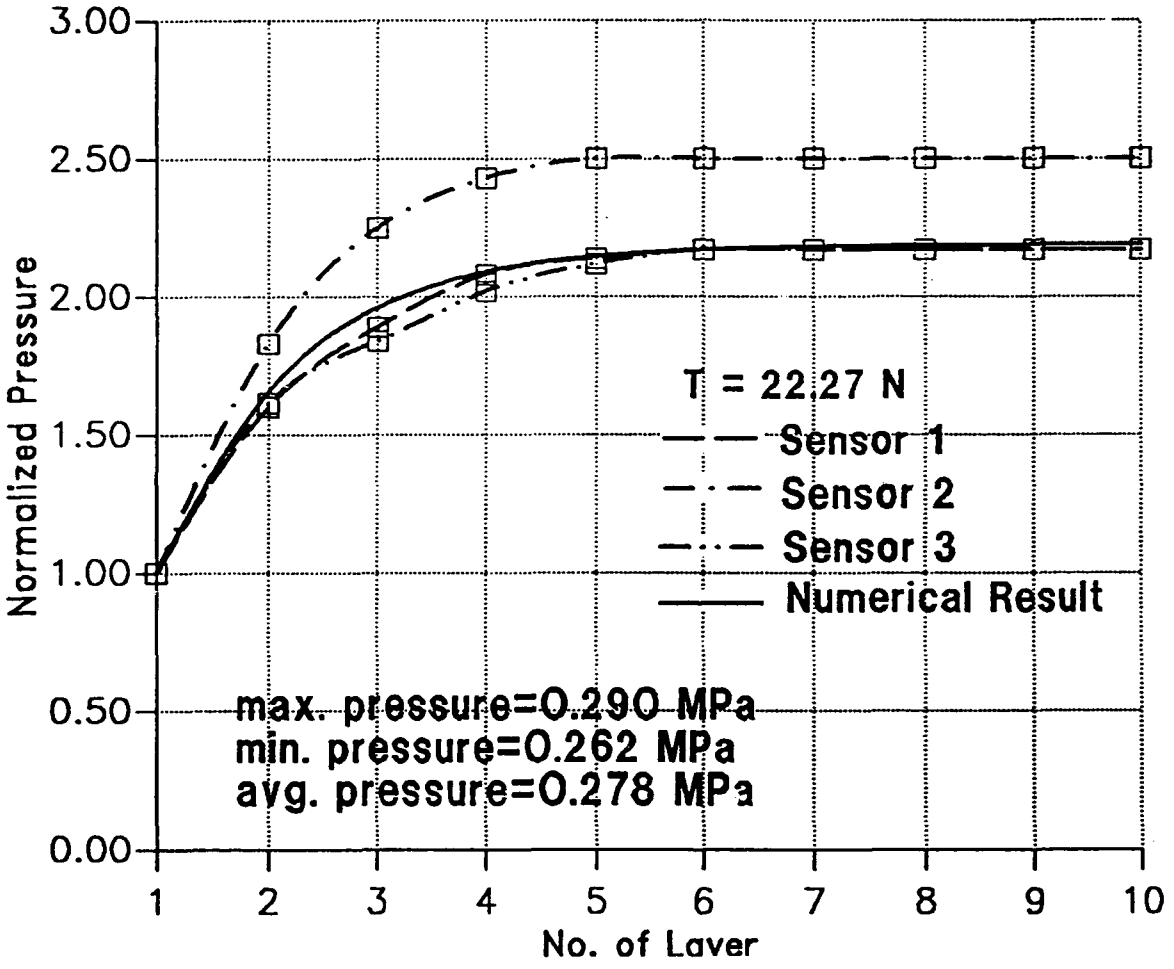

Fig. 13. Change of normalized mandrel pressure with number of layers wound, winding tension = 22.27 N

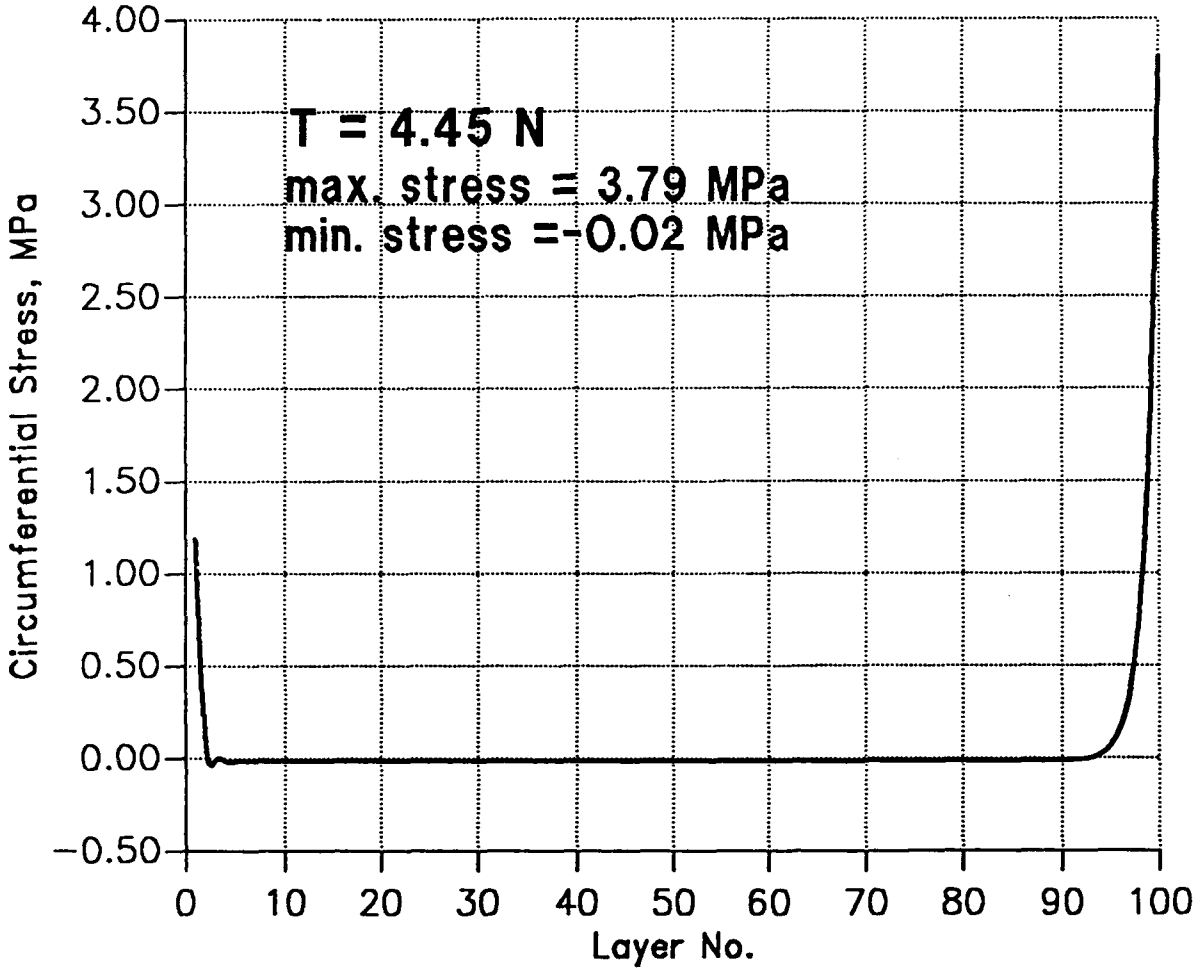

Fig. 14. Circumferential distribution in a 100-layer cylinder, winding tension = 4.45 N

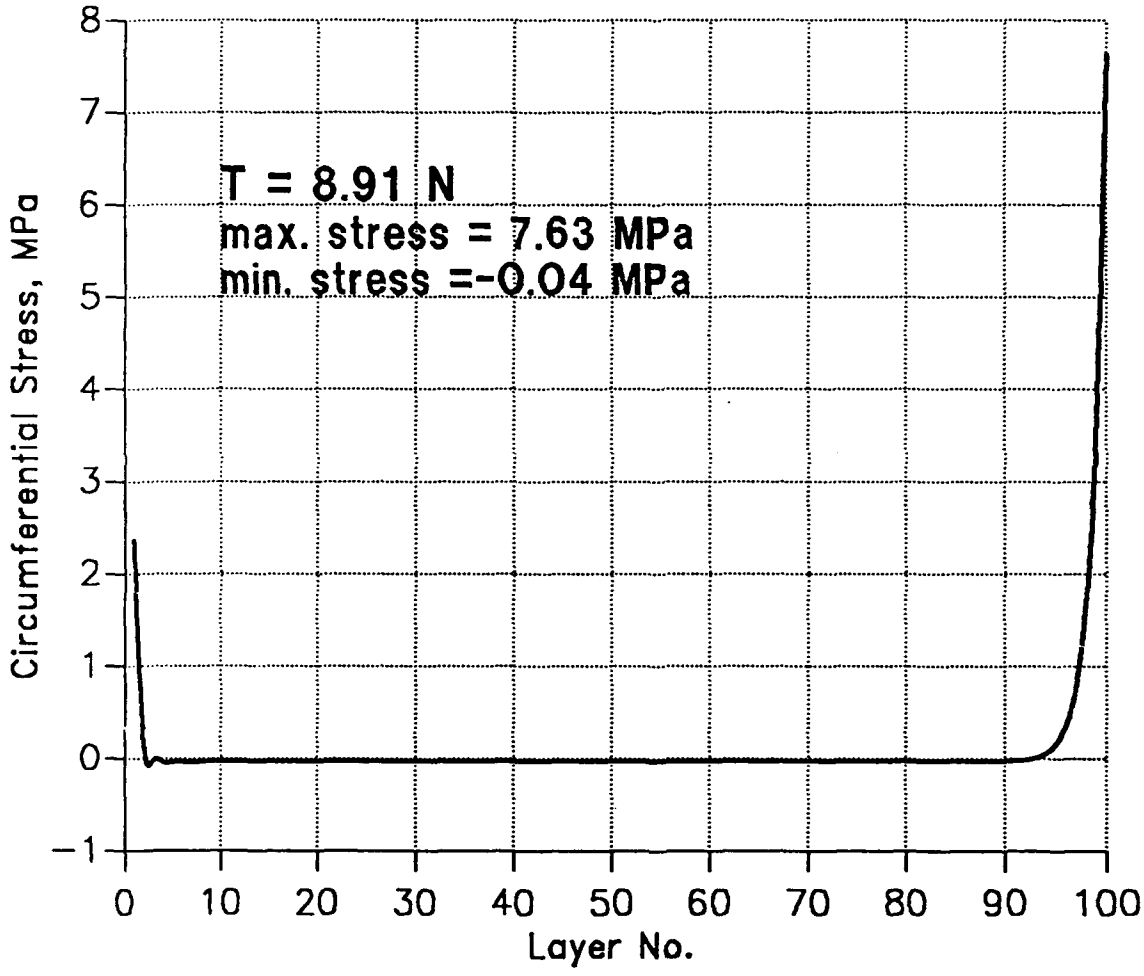

Fig. 15. Circumferential distribution in a 100-layer cylinder, winding tension = 8.91 N

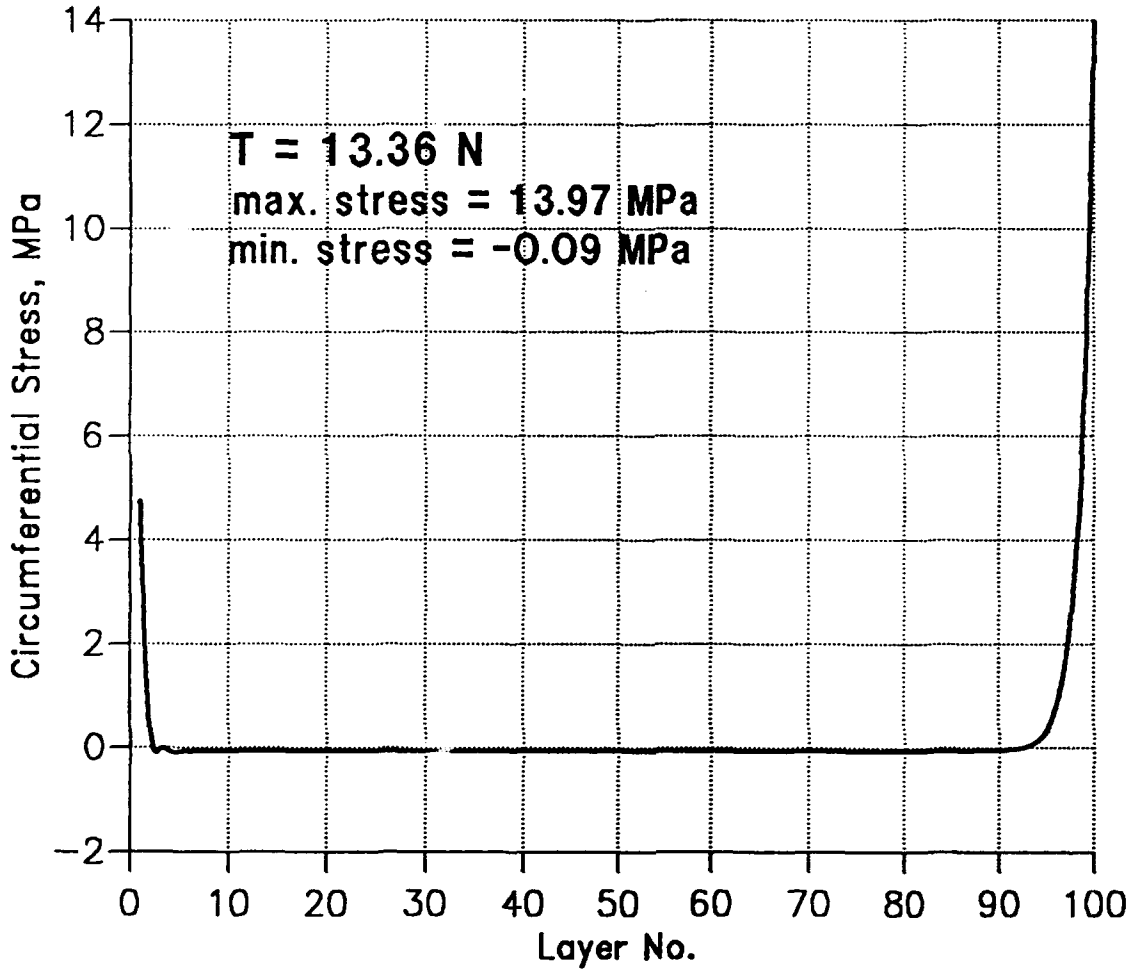

Fig. 16. Circumferential distribution in a 100-layer cylinder, winding tension = 13.36 N

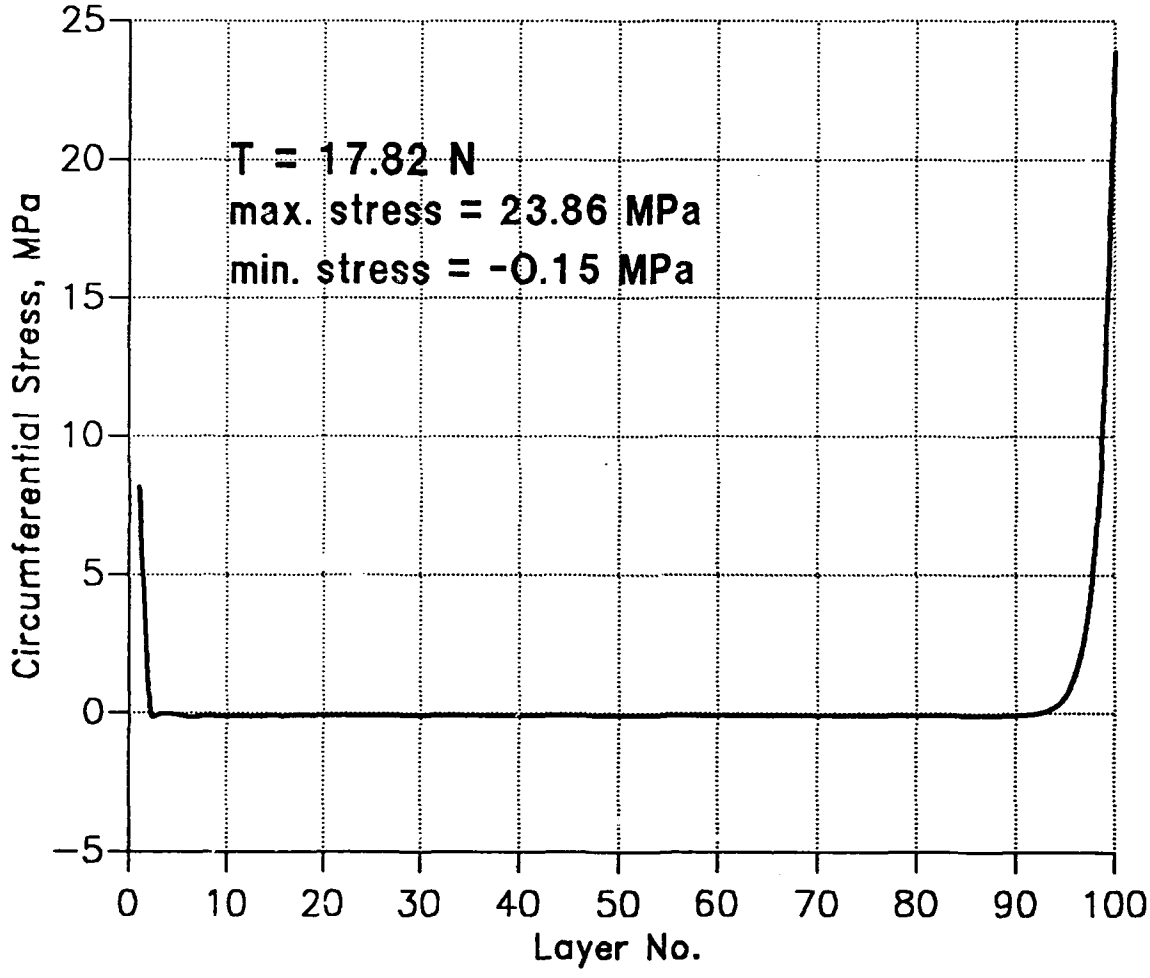

Fig. 17. Circumferential distribution in a 100-layer cylinder, winding tension = 17.82 N

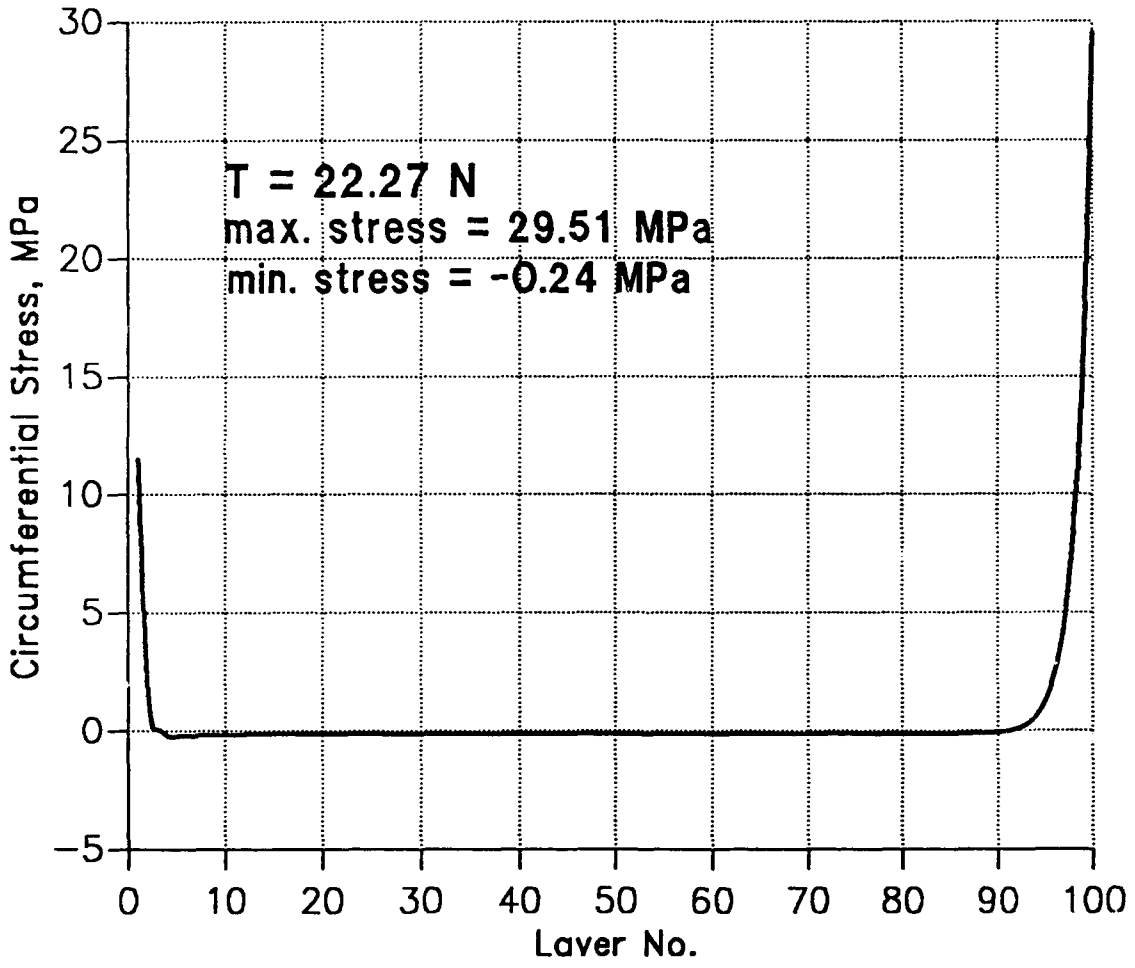

Fig. 18. Circumferential distribution in a 100-layer cylinder, winding tension = 22.27 N

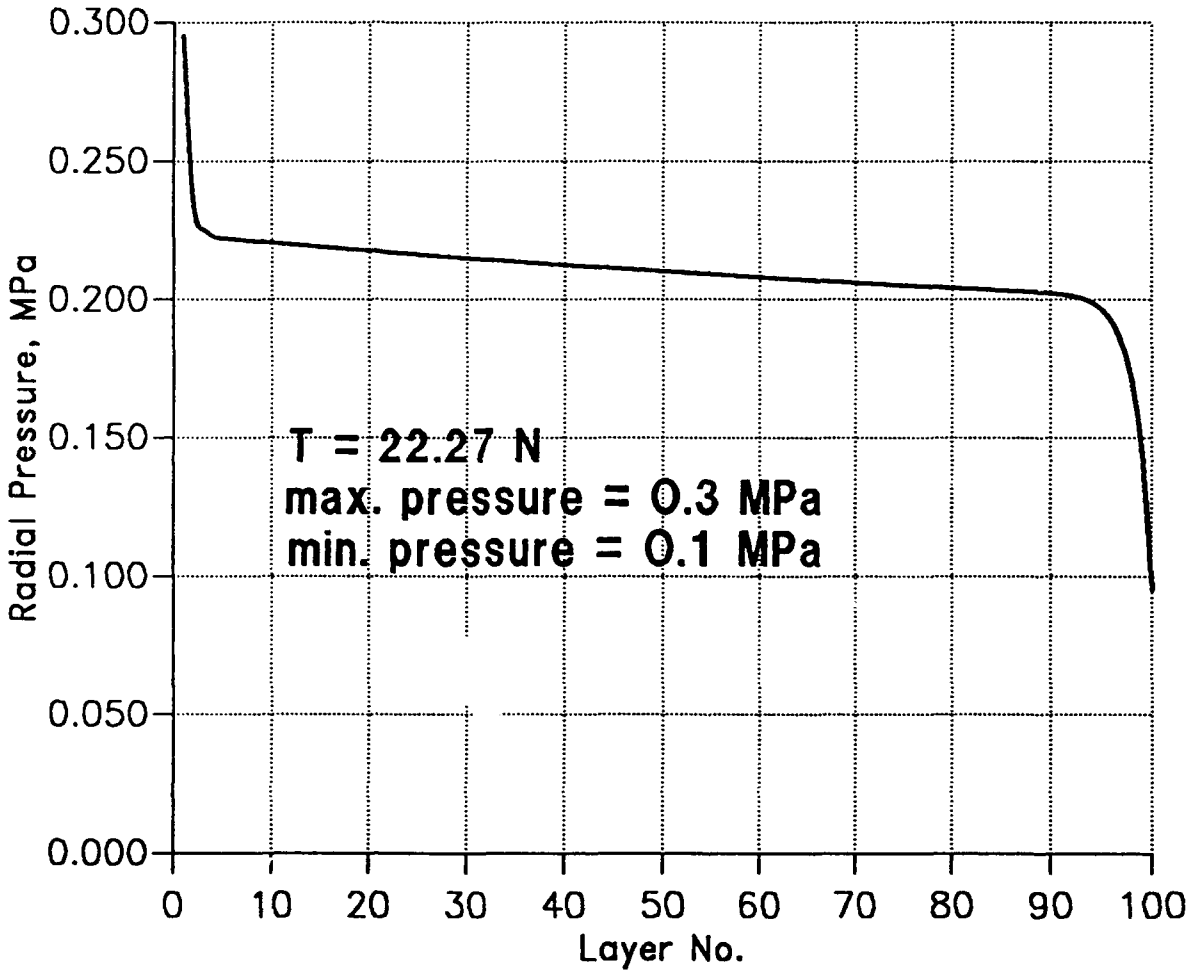

Fig. 19. Radial pressure distribution in a 100-layer cylinder, winding tension = 22.27 N

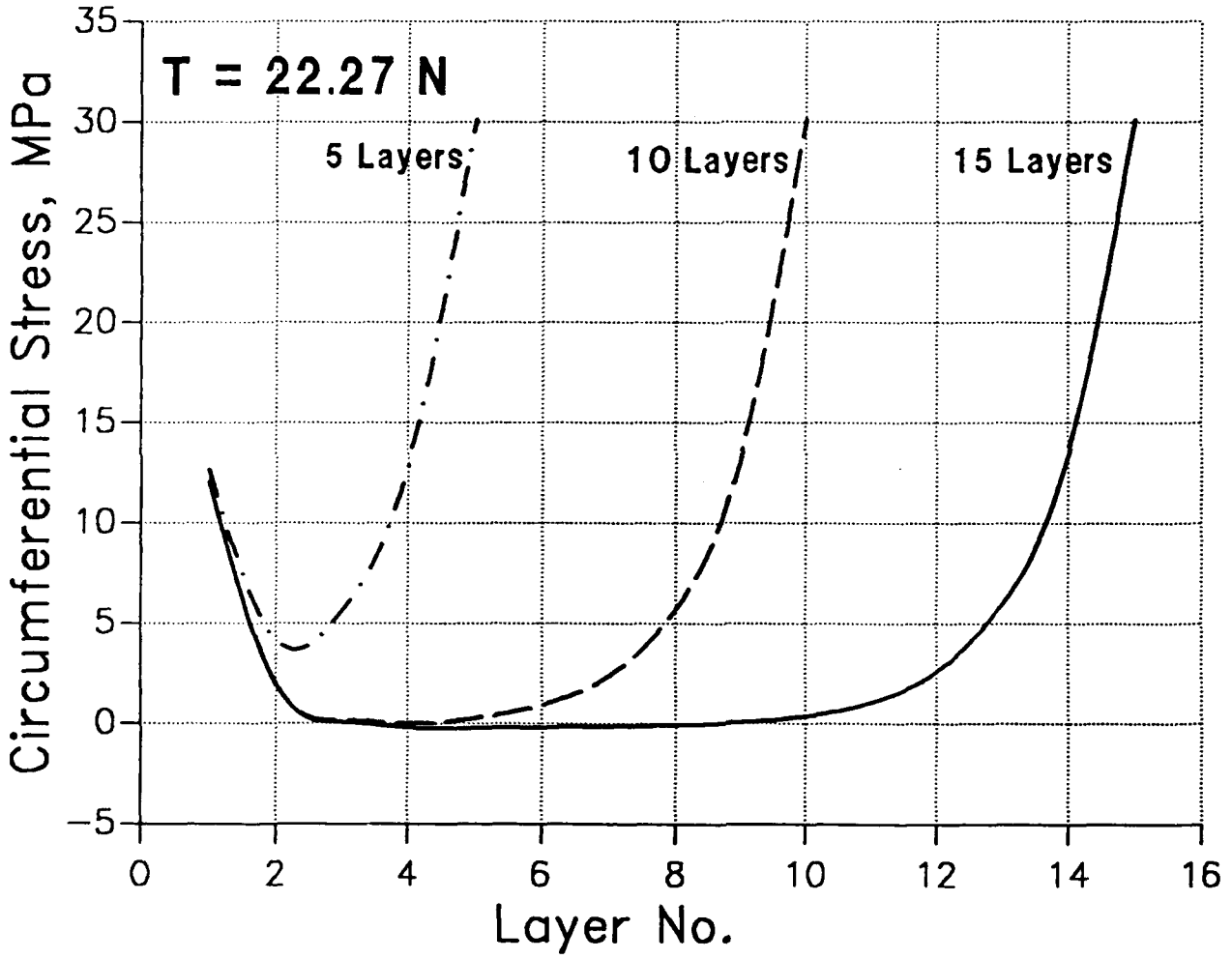

Fig. 20. Change of circumferential stress distribution with number of layers in a cylinder